THE JOURNAL OF PHYSICAL CHEMISTRY B

Article

pubs.acs.org/JPCB

Differential Hydration of Tricyanomethanide Observed by Time Resolved Vibrational Spectroscopy

Daniel G. Kuroda,[†] Prabhat K. Singh,[†,‡] and Robin M. Hochstrasser*

Ultrafast Optical Processes Laboratory, Department of Chemistry, University of Pennsylvania, Philadelphia, Pennsylvania 19104, United States

Supporting Information

ABSTRACT: The degenerate transition corresponding to asymmetric stretches of the D_{3h} tricyanomethanide anion, $C(CN)_3^-$, in aqueous solution was investigated by linear FTIR spectroscopy, femtosecond pump−probe spectroscopy, and 2D IR spectroscopy. Time resolved vibrational spectroscopy shows that water induces vibrational energy transfer between the degenerate asymmetric stretch modes of tricyanomethanide. The frequency−frequency correlation function and the vibrational energy transfer show two significantly different ultrafast time scales. The system is modeled with molecular dynamics simulations and ab initio calculations. A new model for theoretically describing the vibrational dynamics of a degenerate transition is presented. Microscopic models, where water interacts axially and radially with the ion, are suggested for the transition dipole reorientation mechanism.

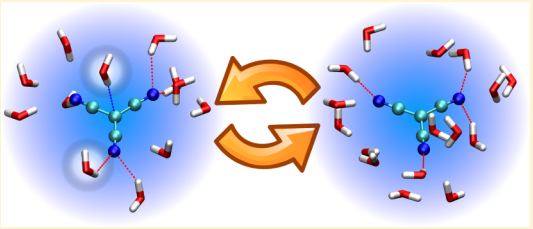

INTRODUCTION

Recently the tricyanomethanide (TCM^-) ion has become the focus of extensive research because of its possible application in ionic liquids (IL). The TCM^- ion forms ILs with very low melting point and viscosity.[1,2] These two characteristics have been key for the successful application of the TCM^- based ILs in batteries and fuel cells.[3] In particular, the mobility of the ions in the IL is essential for characterizing the conductive properties of ILs. However, the use of ions present in the IL as probes to measure its mobility remains relatively unexplored.

The TCM^- ion is a highly symmetric anion composed of three cyano groups attached to a center carbon (Figure 1). The isolated TCM^- ion has three CN groups arranged in D_{3h} symmetry which generates three infrared modes in the CN stretch region. Due to symmetry considerations, two of these three modes belong to a degenerate level which corresponds to a pair of asymmetric stretch transitions (A1 and A2 modes in Figure 2). The remaining mode forms the symmetric stretch (S mode in Figure 2). The degenerate mode is IR active and its transition is located at 2172 cm^{-1}, whereas the symmetric stretching mode is IR inactive and has been observed through Raman spectroscopy at 2225 cm^{-1}.[4,5] Since the TCM^- ion has a well separated and strong absorption in the infrared region of the CN stretch (~2200 cm^{-1}), it is an ideal candidate for

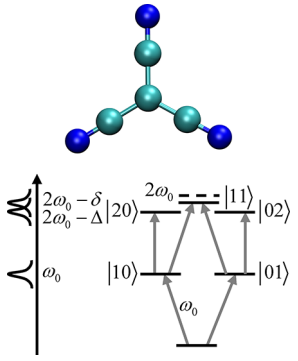

Figure 1. Structure and diagram of the energy levels of the TCM^- ion. In the energy diagram, ω_0 (2172 cm^{-1}) is the center frequency of the degenerate level and Δ (18 cm^{-1}) and δ (9 cm^{-1}) are the diagonal and off-diagonal anharmonicities, respectively.

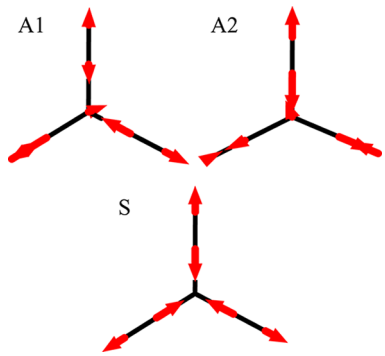

Figure 2. Asymmetric (A1 and A2) and symmetric (S) vibrational modes of the TCM^- ion. The atomic displacements are represented with red arrows.

Special Issue: Paul F. Barbara Memorial Issue

Received: July 12, 2012
Revised: August 29, 2012
Published: August 30, 2012

probing the solvation dynamics of ionic liquids. In addition, the IR active band of the CN stretch region is composed of a degenerate level which makes the TCM^- ion an ideal probe to examine asymmetric solvation perturbation dynamics.

Previous examples of symmetric ions with degenerate transitions used to study solvation dynamics includes oxalate dianion (OXA)[6,9] and guanidinium cation (Gdm^+).[7,8] Gdm^+ is $C(NH_2)_3^+$ which has three equivalent planar C−N groups. The OXA has D_{2d} symmetry with the CO_2^- group plane of $[O2CCO_2]^{2-}$ being perpendicular. In these systems, the structure[7−9] and/or composition[6] of the solvation shell leads to the lowering of the symmetry of the ion producing a splitting of degenerate states. The splitting of the degeneracy and the properties of the resulting eigenstates create a very sensitive probe. This enhanced sensitivity over that from experiments on nondegenerate transitions of a less symmetric ion gives direct information on the solvation shell structure, composition, and dynamics. In particular, it has been shown for the Gdm^+ that the solvent fluctuations induce a lowering of the symmetry, splitting the degenerate level into a pair of distinguishable states. Simultaneously the solvent interactions induces energy transfer between the modes on a subpicosecond time scale.[8] However, due to the spatial overlapping of the modes of Gdm^+ the underlying molecular mechanism responsible for this energy transfer has remained hard to establish. Thus, the study of TCM^- ion is motivated by its possible use as a solvation probe, and it may allow us to gain insights into the hydration processes affecting the vibrational dynamics of more complex yet highly symmetric ions such as the Gdm^+ ion. Another interest is in the water induced vibrational dynamics of the ion that is tracked by measurements of the pump−probe anisotropy as recently demonstrated for oxalate[9] with D_{2d} symmetry and Gdm^+ which has D_{3h} symmetry.[8] In a recent report, Owrutsky and co-workers have reported transient infrared studies of TCM^- ion which included measurements of the energy relaxation time of $V = 1$ state and a suggestion that the pump−probe anisotropy must decay much more quickly than the rotational diffusion.[4] Other vibrational pump−probe measurements on highly symmetric molecules include those on the triply degenerate states of ferric and ferro-hexacyanide[10] and tungsten hexacarbonyl[11] where both have been shown to have initial pump−probe anisotropies of approximately 0.4 that decay rapidly.

In this paper, we investigate the effect of solvent on the vibrational frequency distribution and dynamics of this nearly degenerate level of the TCM^- ion at 2172 cm^{-1}. For this purpose, we use femtosecond IR pump−probe and 2D IR in combination with linear FTIR spectroscopy. Furthermore, molecular dynamics simulations and ab initio calculations have been used to obtain theoretical predictions that enable a molecular picture of the vibrational dynamics of the ion to be obtained.

EXPERIMENTAL AND THEORETICAL METHODS

Experimental Methodologies. Potassium tricyanomethanide (KTCM, 99%) was purchased from Alfa Aesar and was used as received. A 0.1 M solution of KTCM in water was used for all of the experiments. Samples were held between two CaF_2 plates separated by a 6 μm spacer. Linear FTIR spectra were obtained with a Thermo Nicolet 6700 FTIR spectrometer having 0.5 cm^{-1} resolution. All of the measurements were done at room temperature.

Pump−Probe Spectroscopy. The details of the ultrafast laser system used for the experiment have been previously described.[7] In brief the frequency selective pump−probe experiment was based on the generation of femtosecond laser pulses in the 4.5 μm region from an IR optical parametric amplifier (OPA) pumped with a Ti:sapphire based commercial regenerative amplifier (Spitfire, Spectra-Physics). The source generates near transform limited 75 fs pulses centered at 2170 cm^{-1} with ∼2.5 μJ energy. The output was divided into pump and probe pulses. The pump pulse was vertically polarized and contained ∼500 nJ energy at the sample. An attenuator composed of two polarizers was used to decrease the intensity of the probe to ∼50 nJ and to rotate its polarization by 45° with respect to that of the pump pulse. The pulses were focused on the sample to a spot size of less than 200 μm using a parabolic mirror. After the sample the probe beam was collimated and focused onto the entrance slit of a spectrometer and spectrally dispersed with a 100 grooves/mm grating onto a liquid-nitrogen-cooled 32 element MCT array detector. To select parallel, perpendicular, and magic angle polarization components of the probe pulse, a polarizer was placed after the sample. The delay between the pump and probe was controlled by a computer controlled translation stage.

2D IR Spectroscopy. A detailed description of the 2D IR photon echo experiment and methods of data processing have been discussed in detail in an earlier publication.[12] Briefly, a Ti:sapphire amplifier is used to generate Fourier transform limited infrared pulses in a homemade OPA coupled with a difference frequency generator. The IR source consisting of 80 fs duration pulses centered at 2170 cm^{-1} with 400 nJ energy is split into three replicas (wave-vectors: $\mathbf{k}_1$, $\mathbf{k}_2$, and $\mathbf{k}_3$) and focused at the sample using the box configuration geometry. The interaction of the sample with the IR pulses produces a photon echo signal in the phase matching direction ($-\mathbf{k}_1 + \mathbf{k}_2 + \mathbf{k}_3$) and is detected by heterodyning it with a fourth IR pulse (LO) followed by dispersion by a monochromator (100 grooves/mm) onto a liquid-nitrogen-cooled 64 element MCT array detector. In all of the experiments, LO preceded the signal field by ∼1 ps. Two time sequence of pulses, each with a set of specific polarizations of the IR pulses, were used to obtain the corresponding two-dimensional spectra. A rephasing echo signal was produced when the pulses with the wave vector $\mathbf{k}_1$ arrived at the sample before those with wave vector $\mathbf{k}_2$, whereas the nonrephasing spectrum is generated with a time inverted sequence of pulses, i.e., $\mathbf{k}_2$ arrives before $\mathbf{k}_1$. In both sequences, the coherence time interval τ between $\mathbf{k}_1$ and $\mathbf{k}_2$ was scanned with a 2 fs step. The time interval between second and third pulse was varied in steps of 250 fs from 0 to 3 ps to obtain the dependence of the photon echo signal on population time, T. The Fourier transformation of the signal along the coherence, τ and the detection, t axes yields two-dimensional spectrum which measures the correlation between the frequencies ω_τ and ω_t of the coherences that evolve during the τ and t intervals.

THEORETICAL METHODOLOGIES

Molecular Dynamics. The molecular dynamics simulations were performed using the SANDER module of the AMBER 11 program package.[13] A quantum mechanics/molecular mechanics method was used to model the system. The TCM^- ion structure was parametrized according to parametrized model number 3 (PM3) semiempirical formalism and the water was modeled classically with the transferable intermolecular potential 3P (TIP3P) force field. The system consisted of the

dx.doi.org/10.1021/jp3069333 | J. Phys. Chem. B 2013, 117, 4354−4364

TCM^- ion embedded in a 35 Å cube containing ~1400 water molecules. Periodic boundary conditions were imposed in the simulation. Particle-mesh Ewald methodology was used for long-range electrostatic interactions with a cutoff of 12 Å. The SHAKE algorithm was used to fix the bonds involving hydrogen. The simulation was initiated using an initial geometry for the TCM^- ion obtained from the ab initio calculations. The system was energy-minimized for 200 steps using the steepest descent method followed by 300 steps with the conjugate gradient method. Subsequently, the system was equilibrated at a normal pressure and temperature (NPT) for 1 ns with a 2 fs step. Finally, a production run at NPT was recorded for 500 ps extracting snapshots every 2 fs. All simulations used a Langevin thermostat for temperature control.

Ab Initio Calculations. DFT calculations were performed at the B3LYP/6-31+G** (ab initio) and PM3 (semiempirical) level using the Gaussian 09 software package.

Determination of Frequency Evolution of Degenerate Modes. The TCM^- ion in water has a nearly degenerate level whose component states interconvert over the MD trajectory (time). To follow the time evolution of a particular mode of this degenerate level, the following methodology was used. The coordinates of only the TCM^- ion were extracted from the MD trajectory every 4 fs. These sets of coordinates were used for calculating the instantaneous normal modes and normal mode displacements using PM3 level theoretical calculations. From the instantaneous normal modes calculations, the two frequencies (ω_1 and ω_2) corresponding to the A1 and A2 modes were extracted and labeled according to their frequency such that $\omega_1 < \omega_2$. By comparing the associated set of atomic displacement vectors of each frequency in two consecutive MD snapshots, a similarity factor defined as the sum of the difference squared of the displacement vectors was calculated (eq 1).

$$F_{\text{sim}} = \sum_{i,j}\sum_{a=1}^{7} (x_a^i(n) - x_a^j(n+1))^2 + (y_a^i(n) - y_a^j(n+1))^2 + (z_a^i(n) - z_a^j(n+1))^2 \quad (1)$$

In eq 1, F_{sim} is the similarity factor, and $\{x_a^i(n), y_a^i(n), z_a^i(n)\}$ are the displacement coordinates for the ath atom in the ith normal mode in the nth snapshot. The similarity factor was computed for the cases in which the normal mode with the lowest and highest frequency maintains its frequency order ($i = j$) or it changes ($i \neq j$). Thus if $F_{\text{sim}}(i = j) < F_{\text{sim}}(i \neq j)$, the frequency of the normal mode is considered to be unchanged in the successive snapshot (e.g., $\omega_1(n) \rightarrow \omega_1(n+1)$), otherwise if $F_{\text{sim}}(i = j) > F_{\text{sim}}(i \neq j)$, a change in the frequency of the normal mode have occurred (e.g., $\omega_1(n) \rightarrow \omega_2(n+1)$). The presented methodology allows one to tag the switch of the normal-mode frequencies of a degenerate level by following the evolution of the normal mode displacements.

Normal Mode Analysis. In the MD simulation, the instantaneous conformation of an ion is characterized by a set of displacement coordinates.[14] These displacement coordinates, when freed from overall translational and rotational motions, can be represented by a linear combination of displacement vectors of normal mode eigenvectors. The normal mode coordinates are defined at some instant of time t as

$$Q_i(t) = \sum_{i=1}^{3N} c_{ai} q_a(t) \quad (2)$$

where q_a are the mass-weighted Cartesian displacement coordinates for the ath atom and c_{ai} are dimensionless coefficients for the ath atom in the ith normal mode. The summation extends over the $3N$ mass weighted displacement coordinates of the ion. Eigenvectors are orthonormalized as follows:

$$\sum_{a=1}^{3N} c_{ai} c_{aj} = \delta_{ij} \quad (3)$$

The normal mode coordinates ($Q_i(t)$ in eq 2) can be calculated by replacing $q_a(t)$ with $(m_a)^{1/2} r_a(t)$ where $r_a(t)$ is the displacement of the ath atom at time t observed in the MD simulation. To obtain the $Q_i(t)$ from the MD simulation, in each snapshot of the trajectory the atomic coordinates of the TCM^- are "aligned" via root mean squared minimization to the atomic coordinates and center of mass of the system in the minimum of energy. This "alignment" procedure removes the overall translation and rotation of the ion that occurs along the MD trajectory.[15] The remaining atomic displacements with respect to the conformation with minimum energy, $r_a(t) = r_a^{E_{\min}} + \Delta r_a(t)$, are used to calculate the $Q_i(t)$ from eq 2. The normal mode eigenvectors (c_{ai}) necessary in eq 2 are directly computed from ab initio calculations. Although there are 3N normal mode eigenvectors in eq 2, there are only 3N-6 normal mode coordinates ($Q_i(t)$) because the displacements ($\Delta r_a(t)$) are freed from rotational and translational motions by rmsd fitting, thereby making the normal mode coordinates for these type of motions zero.

RESULTS

The FTIR spectrum of 0.1 M TCM^- ion in water presents an absorption band in the 2100−2250 cm^{-1} region (Figure 3). It

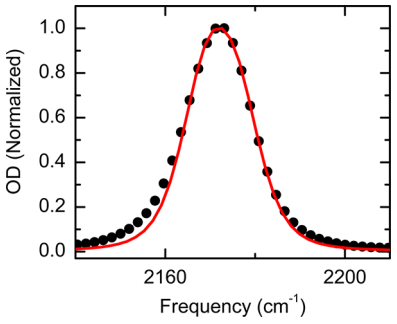

Figure 3. Normalized FTIR spectra of 0.1 M solution of TCM^- ion in water with solvent background subtracted. The solid circles represent the experimental data points, whereas the solid line (red) represents the simulated FTIR spectra using the parameters listed in Table 1.

has been reported that the TCM^- ion derives from a super acid ($pK_a = -5$).[16] The spectrum is that of the isolated anion as proved by its concentration independence down to 0.005 M (not shown here). This peak at 2172 cm^{-1} is located atop the broad and weak combination band of water. It corresponds to the degenerate asymmetric stretch mode of the TCM^- ion.[4] The peak molar absorptivity and bandwidth at half-maximum of this degenerate transition are $\varepsilon = 4383 \pm 50$ M^{-1} cm^{-1} and fwhm = 18 cm^{-1}, respectively. This absorption band is not well

dx.doi.org/10.1021/jp3069333 | J. Phys. Chem. B 2013, 117, 4354−4364

described either by a single Gaussian or by a single Lorentzian line shape. Fitting to a Voigt profile yields Gaussian and Lorentzian components of 13 and 8 cm^{-1}, respectively. None of the simple functions give excellent fits because the absorption band is asymmetric, being broadened on the low frequency side (see Figure 3). Moreover the band is expected to consist of two components of a degenerate level. The spectrum would appear to be only one transition only if the degeneracy were not split by the interactions with solvent molecules. The absorption band is modeled quite well with the parameters used for simulation of 2DIR spectra (Table 1, see below).

Table 1. Parameters Used for Simulation of 2D IR Absorptive Spectra

	transition	
parameters	1	2
ω, cm^{-1}	2169	2176
Δ_1, cm^{-1}	18	18
Δ_σ, cm^{-1}	9	9
μ	1.0	
$D_{\|}$, $D_\perp \times 10^{10}$ s^{-1}	6.4	
K_{et}, ps^{-1}	0.6	
$\langle \delta\omega_i(t)\ \delta\omega_i(0)\rangle$		
Δ, ps^{-1}	1.1	
τ_σ, ps	1.2	
$\langle \delta\omega_i(t)\ \delta\omega_j(0)\rangle$		
Δ, ps^{-1}	1.1	
τ_σ, ps	1.2	

The spectral response of the TCM^- ion in water after excitation with an intense pulse centered at ~2170 cm^{-1} is shown in Figure 4 in which the signals from the neat solvent

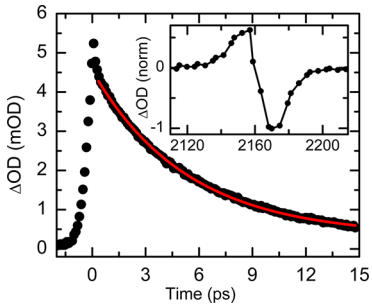

Figure 4. Bleach signal for the TCM^- ion at 2172 cm^{-1}. The filled circles are the experimental data points, and the red line is the single exponential fit. Inset: Experimental pump–probe spectra of 0.1 M TCM^- ion in water at T = 0.3 ps.

have been subtracted from the pump–probe data sets. The pump–probe spectrum at T = 0.3 ps (inset, Figure 4) shows a negative band which corresponds to the V = 0 to 1 transition (bleach of the ground state and stimulated emission) and a positive band which is assigned to the V = 1 to 2 transition (excited state absorption). The new absorption and bleach bands are separated by 22 cm^{-1} due to anharmonicity and the band shape of overlapping transitions. The dynamics of the transient bleach signal is presented in Figure 4. When the first 0.2 ps of the signal is omitted to avoid contamination by nonresonant signals, the response can be modeled with a single exponential decay having a time constant of 5.3 ± 0.1 ps. A similar analysis of the transient photoinduced absorption signal yields 4.8 ± 0.1 ps (see the Supporting Information). These results are in good agreement with the previously reported value.[4] In addition, analysis of the parallel ($I_{\|}$) and perpendicular ($I_\perp$) components of the photoinduced absorption band show that the anisotropy of this transition has a fast decay. The anisotropy defined as

$$r(t) = (I_{\|}(t) - I_\perp(t))/(I_{\|}(t) + 2I_\perp(t))$$

is represented in Figure 5. The dynamics of the TCM^- ion anisotropy is well represented with a double exponential decay

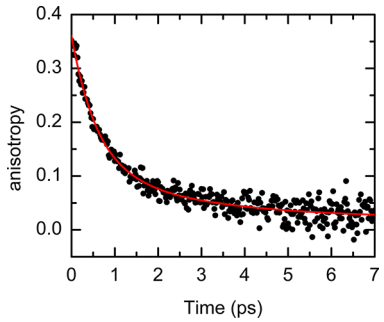

Figure 5. Anisotropy decay at excited state absorption band (2152 cm^{-1}).

function ($r(t) = A_f e^{-t/\tau_f} + A_s e^{-t/\tau_s}$) with two well separated time constants. The anisotropy components have decay time constants (amplitudes) of 0.58 ± 0.08 ps (A_f = 0.24 ± 0.04) and 2.6 ± 1.1 ps (A_s = 0.12 ± 0.03), respectively. Although neither the population nor the anisotropy have a significant dependence of their characteristic times on the detected infrared frequencies (see the Supporting Information), the amplitudes of the components of the pump–probe anisotropy are frequency dependent. The total amplitude of the anisotropy at T = 0 is 0.29 at the bleach/stimulated emission band whereas it is 0.36 at the position of the transient absorption.

The 2D IR spectra of the TCM^- ion in water were also investigated, and they are shown in Figure 6 at different waiting times, T. At T = 0, the 2D IR spectrum is composed of two peaks (negative and positive). The positive peak (red peak, Figure 6) corresponds to the excited state absorption, whereas the negative peak (blue peak, Figure 6) is caused by the bleach of the ground state and stimulated emission. While both peaks are elongated along the diagonal (dashed line), the positive peak is significantly more stretched along the ω_t axis compared with the negative peak. As the waiting time increases, the spectrum becomes more upright with the peaks more elongated along ω_τ. Furthermore, at later waiting time the initially elongated peaks appear to acquire a "square-like" shape. Moreover, the signal in a slice passing through ω = 2176 cm^{-1} and perpendicular to the diagonal trace of the 2D IR spectrum shows that the low and high frequency sides of the main peak ($\omega_\tau = \omega_t$ = 2176 cm^{-1}) grow with waiting time as seen in Figure 7. The vibrational lifetime dependence is removed from the data in Figure 7 by normalizing to the maximum of the diagonal spectrum. The modeling of this growth of the high frequency side shows a time constant of 0.6 ps (see below). The change of peak geometry from "elliptical" to "square-like" and the growth of off-diagonal spectral components are an indication of the 2D IR spectrum being composed of two closely lying transitions with cross-peaks as will be shown later.

dx.doi.org/10.1021/jp3069333 | J. Phys. Chem. B 2013, 117, 4354–4364

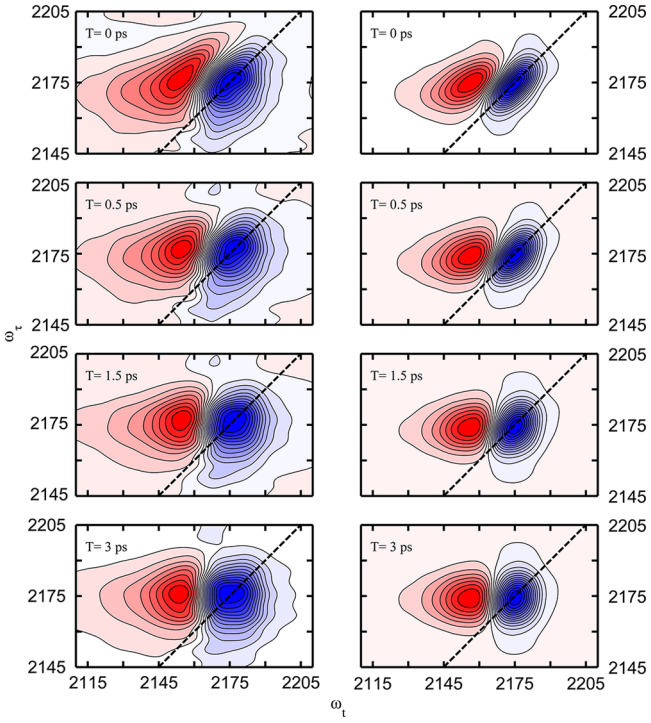

Figure 6. Absorptive 2D IR spectra of TCM^- ion in water. Experimental (left column) and simulated (right column) 2D IR spectra at different waiting times: T = 0, 0.5, 1.5, and 3 ps.

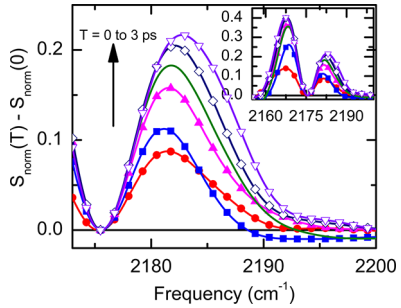

Figure 7. Signal in a slice passing through ω = 2176 cm^{-1} and perpendicular to the diagonal trace of the 2D IR spectrum at different waiting times (T), 0, 0.5, 1.0, 1.5, 2.0, 2.5, and 3 ps after lifetime dependence removal (S_{norm}) and subtraction of the signal at T = 0. Inset shows the entire spectral region.

DISCUSSION

Energy Levels of the TCM^- Ion. A probable vibrational energy level diagram in the V = 0, 1, and 2 region for TCM^- is presented in Figure 1. Although FTIR, pump–probe, and 2D IR spectroscopy can be used to obtain the frequencies of the one quantum transitions ($|0\rangle$ to $|01\rangle/|10\rangle$) and the two quantum transitions ($|01\rangle$ to $|02\rangle$ or $|10\rangle$ to $|20\rangle$), the frequency position of the combination mode ($|11\rangle$) has not proved to be obtainable from these measurements. However, the combination mode location can be obtained from the pump–probe anisotropy at zero delay time. The pump–probe anisotropy at T = 0 is the sum of all of the Liouville pathways[17] that contribute to the stimulated emission, coherence, excited state absorption, and bleaching signals.[18] Neglecting any interstate dynamics, and assuming all the transition dipoles are given as the values for harmonic oscillators, the pump–probe anisotropy at T = 0 for a 2-fold degenerate vibration is given by

$$r(\omega) = [0.9S_F(\omega_0 - \omega) - 0.1S_C(\omega_0 - \delta - \omega) - 0.4S_D(\omega_0 - \Delta - \omega)]/[3S_F(\omega_0 - \omega) - S_C(\omega_0 - \delta - \omega) - S_D(\omega_0 - \Delta - \omega)] \quad (4)$$

where S_F, S_C, and S_D are the spectral shape factors, normalized to unity on ω, of the signal arising from bleach and stimulated emission (F), combination mode (C), and new absorption bands (D), respectively. The lineshapes represented by these S factors are defined by the parameters of system, such as correlation functions, lifetimes, etc., and the peak frequencies are determined by the frequency of the one quantum state, ω_0, the diagonal anharmonicity, Δ, and the off-diagonal anharmonicity, δ. This equation is a formal representation of the procedure we have used for fitting the anisotropy for transitions to a degenerate level.[7,18]

Equation 4 shows very clearly that, if the new absorption, combination mode, and bleach/stimulated emission signals are not overlapping, the pump–probe anisotropies at zero delay time in the regions of the new absorption signals are 0.4 and that in the bleach/stimulated emission region is 0.3. The isolated combination mode transition presents an anisotropy of 0.1. If the bleach/stimulated emission and combination mode contribution are not spectrally separated, the anisotropy is 0.4. This latter value is the most common result for vibrations where it is often found that the spectral line width is larger than δ. In any event the anisotropy near T = 0 is not a canonical number such as the 0.4 expected for nondegenerate transitions but it is expected to lie anywhere between 0.3 and 0.4. Furthermore the anisotropy is expected to be frequency dependent. It is also apparent that a very broad band pump–probe anisotropy would encompass all of the terms in eq 4 to yield 0.4, as is found for nondegenerate transitions. TCM^- has experimental zero delay pump–probe anisotropy values of 0.36 in the new absorption and 0.29 in the stimulated emission/bleach bands. These results are very close to expectations from eq 4 if the off-diagonal anharmonicity plays no role. It follows that the location of the TCM^- combination mode $|11\rangle$ is expected to be in a region of the spectrum where it has little or no effect on either new absorption or bleach/stimulated emission anisotropies. Since the diagonal anharmonicity and the full width at half-maximum of the absorption band are both 18 cm^{-1}, it is likely that the combination mode band is located close to halfway between the bleach and new absorption signals. This would require that δ = 9 cm^{-1}. For these parameters and assuming that all of the spectral factors are Gaussian functions with a fwhm of 18 cm^{-1}, our model gives qualitative agreement with experimental values. However, to produce a more quantitative estimate of the off-diagonal anharmonicity one would require to obtain a more accurate spectral shape factors for the bleach/stimulated emission, combination and new absorption bands (S_F, S_C, and S_D in eq 4).

Dipole Reorientation Mechanism. The time dependence of the anisotropy of the transient absorption signal of the TCM^- ion is well represented by a double exponential decay with subpicosecond and picosecond components having amplitudes of 0.24 and 0.12, respectively. The total anisotropy near T = 0 is 0.36. Many different molecular processes can contribute to the ultrafast dynamics of the anisotropy. Given the small size of the ion, it must be investigated whether a

dx.doi.org/10.1021/jp3069333 | J. Phys. Chem. B 2013, 117, 4354–4364

subpicosecond component could arise from the rotational diffusion of the ion. The dynamical model for the anisotropy observed for the orientational diffusion of an oblate diffusor having the transition dipole located in the same plane as the degenerate principal axes of the oblate ellipsoid is given by

$$r(t) = 0.1\exp(-6D_{\perp}t) + 0.3\exp(-(2D_{\perp} + 4D_{\parallel})t) \quad (5)$$

where $D_{\perp}$ and $D_{\parallel}$ are the rotational diffusion constants. This model predicts the same number of components as that for the experimental anisotropy. The first component of this model decays with a characteristic time of $1/6D_{\perp}$ with an amplitude of 0.1 and the other component has an amplitude of 0.3 with a decay constant of $1/(2D_{\perp} + 4D_{\parallel})$.

The rotational relaxation time τ_R is predicted to be

$$\tau_R = \frac{1}{6D_{\perp}} = \frac{\eta V\lambda}{6k_BT_K} \quad (6)$$

where T_K is the temperature (295 K), k_B is the Boltzmann's constant, η is the viscosity, V is the volume of the molecule, and λ is the friction coefficient. For slip boundary conditions, the friction coefficient is 0.8095,[19,20] which gives a value of τ_R = 3 ps, This value is in reasonable agreement with the slow decay time of 2.6 ps seen in the experiment. The other time constant (with an amplitude of 0.3) is estimated to be 1.41 ps assuming $D_{\parallel}$ is inertial (see the Supporting Information). This value is still much slower than the fast decay component observed in anisotropy. For stick boundary conditions,[21] the two time constants are predicted to be 22.9 ps (amplitude of 0.1) and 25.6 ps (amplitude of 0.3) which are both much slower than the experimentally observed decay time constants (see the Supporting Information). It can be concluded that the ultrafast portion of the dipole reorientation process observed experimentally is not a result of the rotational diffusion of the molecule. However, the 2.6 ps decay of the component with an amplitude of 0.12 is attributed to the orientational diffusion of the ion around the axis perpendicular to the 3-fold symmetry axis. This assignment is confirmed from MD simulations which predict a dipole reorientation of 3.3 ps for the ion in water (see the Supporting Information).

A molecular mechanism of the fast anisotropy decay must involve the solvent induced coupling between the degenerate vibrational modes. Energy transfer between the two component states results in $\pi/2$ jumps in the transition dipole moment without modifying significantly the 3-fold symmetry of the ion. This process can be thought of as the energy transfer from one vibrational mode to another mode that happens to be at essentially the same frequency. The characteristic forward and backward jump times are τ_{et}. If rotational diffusion is neglected, the terms in eq 4 are dependent on the delay time T. Equation 4 is specifically for $T = 0$. For $T \gg \tau_{et}$ the summation of all the contributing Liouville pathways[22] leads to a frequency independent anisotropy of 0.1. This mechanism robustly predicts the residual anisotropy to be 0.1, which is a characteristic of excitation to a degenerate level. The experimental result is in agreement with this assessment in yielding 0.12 ± 0.03 for the limiting anisotropy. This kind of mechanistic information is also encoded in the 2D IR spectra. The 2D IR spectrum contains contributions from different processes such as ground state bleaching and photoinduced absorption. In the presence of population transfer between different transitions during the waiting time, the different contributions to the 2D IR spectrum are affected by the possibility of the population transfer between the two degenerate states. In the proposed dipole reorientation mechanism, cross-peaks between transitions are expected to appear as a consequence of the dynamic exchange that will transfer some of the initial population to a new state. A gradual increase in the cross-peak amplitude with the waiting time has been observed in the experiment and is discussed in the following section. This observation further supports the proposal of solvent induced population transfer as the reason for the fast decay in anisotropy. The transition dipoles associated with the two degenerate modes are perpendicular to each other so the solvent induced interconversion producing 90° jumps will lead to a reorientation of the transition dipole on the time scale of interconversion. Pseudorotation which causes 120° jumps between transition dipoles owing to exchange between structures with equivalent solvent configurations is not considered as a possibility here for the fast dipole reorientation. In the case of the analogous Gdm^+ ion,[8] the pseudorotation was found to be much slower than the subpicosecond time scale.

Population Transfer. It is common that the improved resolution of 2D IR over conventional FTIR can allow the resolution of otherwise overlapping transitions.[6,23] The 2D IR spectra of the TCM^- ion in water even at large values of T when the resolution is optimum[6,24] does not resolve the peak at 2172 cm^{-1} into two components. This result suggests that the water interaction is not sufficiently asymmetric to distort significantly the average ion geometry and that the ion maintains its structure close to 3-fold symmetry. The time evolution of the diagonal trace of the 2D IR spectrum, which shows only a slight narrowing in the width as waiting time (T) increases, further reinforces that the band at 2172 cm^{-1} is the result of a superposition of two very similar inhomogeneously broadened transitions. For a single nondegenerate vibrational mode the 2D IR spectrum becomes circular at very long waiting times.[25−27] However, at large T values the positive peak of the TCM^- ion 2D IR spectrum, rather than becoming circular, adopts a "square-like" shape. Such a shape would be characteristic of two nearby transitions developing cross-peaks even when the cross-peaks are not clearly identifiable because of the very small frequency separation of two component states. Moreover, the time evolution of the signal in a slice perpendicular to the diagonal shows clearly the growth expected from such a cross-peak. This result strongly indicates the presence of population exchange during the waiting time. The evolution of cross-peak amplitude with waiting time was estimated by measuring the ratio of the change in the signal volume at the cross-peak (ω_t = 2183 cm^{-1}, ω_τ = 2176 cm^{-1}, radius = 2 cm^{-1}) and at the diagonal peak (ω_t = 2176 cm^{-1}, ω_τ = 2176 cm^{-1}, radius = 2 cm^{-1}) as a function of waiting time. Figure 8 shows the growth of the change in the ratio of the cross-peak to diagonal peak volumes that occurs between $T = 0$ and T.

To estimate the energy transfer rate constant from the growth in cross-peak amplitude, a 2D IR spectral simulation model for energy transfer between degenerate modes has been employed. The model takes into account the energy transfer between the one-quantum states by allowing spontaneous jumps back and forth between the two states during the waiting time (T). The expression for the ratio of cross-peak to diagonal peak ($S_{12}(T)/S_{22}(T)$) for a pair of nearly degenerate transitions with equal transition dipoles at any waiting time (T) is obtained by adding all of the relevant Liouville pathways.[22] The complete set of pathways and their time dependences are given explicitly

dx.doi.org/10.1021/jp3069333 | J. Phys. Chem. B 2013, 117, 4354−4364

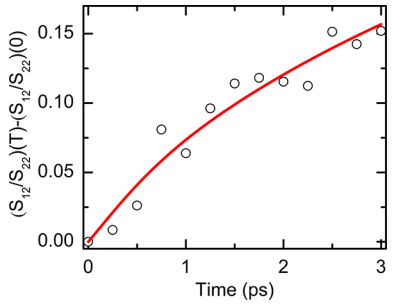

Figure 8. Ratio of the volume of cross-peak to the diagonal peak. The open circles are the data points, and the solid red line is the fit according to eq 7.

in ref 22 where the ratio of cross-peak to diagonal peak signal is given for all four beams having the same polarization, and the combination mode excluded from the signal is given by

$$\frac{S_{12}(T)}{S_{22}(T)} = \frac{2(P_{12}(T) + 1) + e^{-\Gamma T}}{6(P_{11}(T) + 1) + e^{-\Gamma T}} \quad (7)$$

where $P_{12}(T) = (1 - e^{-2k_{et}T})/2$ is the probability that if a molecule is initially in the state $1 = |10\rangle$ at $T = 0$, it will be transferred to the state $2 = |01\rangle$ after a time T. The factor $P_{11}(T)$ is the probability it will not be transferred. The pure dephasing rate of the interstate coherence is Γ, which appears because the $|10\rangle$, $|01\rangle$ coherence pathways contribute to the signal. Figure 8 shows the fitting of the experimental data points according to eq 7. The least-squares fit to the data gives a pure dephasing rate (Γ) of 1/0.01 ps^{-1} and energy transfer rate constant (k_{et}) of 1/0.7 ps^{-1}. A very similar growth of the ratio of the amplitude of the cross-peak to diagonal peak has been obtained using 2D IR spectral simulation (to be discussed later) using an energy transfer rate of 1/0.6 ps^{-1}. The modeling of the cross-peak growth predicts a time constant for the energy transfer of ~0.7 ps which is very similar to the fast dipole reorientation observed in the anisotropy and suggests that solvent induced energy transfer is most likely the mechanism by which the anisotropy is lost.

The energy transfer process considered above can also be regarded as the vibrational energy relaxation between degenerate states. In the context of energy relaxation, the transfer between vibrational modes will be given by the changes in one of the modes that are brought about by fluctuations in the force exerted on the other mode by the solvent. Using the vibrational energy relaxation theory,[28] the rate of transition between two modes, represented by normal coordinates Q_1 and Q_2, is given by

$$k_{et} = \frac{1}{\hbar^2}\int dt\ \langle V_{12}(t)V_{21}(0)\rangle \quad (8)$$

where $V_{12}(t)$ is the fluctuating part of the solvent induced coupling between the modes and is given by

$$V_{12}(t) = \left[\frac{\partial}{\partial Q_1}\left(\frac{\partial V(t)}{\partial Q_2}\right)\right]_0 Q_1Q_2 + \ldots$$
$$= \gamma_{12}(t)Q_1Q_2 + \gamma_{21}(t)Q_1Q_2 + \ldots \quad (9)$$

where $\gamma_{12}(t)$ is the solvent induced force gradient and represents the change in Q_1 due to force exerted by the solvent on Q_2. The angled brackets imply a trace over the bath coordinates. Finally, the rate of energy transfer from one mode to the other in terms of force gradients to a first approximation is given by, $2k_{et} = 1/\omega_0^2\int dt\ \langle\gamma_{12}(t)\gamma_{21}(0)\rangle$. In principle this quantity could be obtained from a classical MD simulation, but we did not proceed in this direction.

Similarly, the terms of eq 8 can be considered as the off-diagonal terms of the density matrix (ρ_{12}) which will be responsible for the equilibration/mixing of the vibrational states originally present in the ion or equivalently the decay/growth of the diagonal terms (ρ_{ii}) in the density matrix. The diagonal terms are represented by $\rho_{ii} = \langle c_i^*(t)c_i(t)\rangle$. These time dependent coefficients represent the way in which states get mixed by interaction with the bath. Similarly the instantaneous normal mode coordinates ($Q_i(t)$ of eq 2) will show the same time dependence since the displacement of the atoms of the ion from its minimum energy conformation is caused by forces exerted by water (bath). Thus the influence of the time varying forces imposed on a particular normal mode will be directly manifested in the value of the instantaneous normal mode coordinates of that particular normal mode as will be observed in the time dependent coefficients ($c_i(t)$) obtained by solving the time dependent Schrodinger equation. The time evolution of the normal mode coordinates ($Q_i(t)$) should provide the same dynamics information as the computation of k_{et} from eq 8.

The dynamics of normal mode coordinates was calculated from the normal-mode analysis of displacement vectors (see the Theoretical Methodologies section). The loss of correlation of the normal mode coordinates provides a quantitative estimate of population transfer (mixing) induced by solvent. Figure 9 shows the autocorrelation of the mode A1 coordinates.

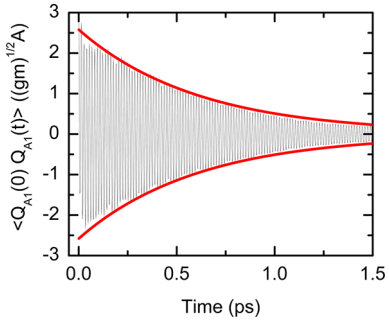

Figure 9. Autocorrelation of normal mode coordinates for mode A1. The red lines are constructed using fitting parameters to help visualize the fitting of the decay of the envelope of the oscillatory correlation function.

The autocorrelation of the normal mode coordinates for both the A1 and A2 normal mode was found to decay with a correlation time of ~0.6 ps. The strong similarity in times scales of the population transfer predicted by normal mode analysis and experimentally observed in 2D IR suggests that the solvent induced population transfer occurs in subpicosecond time scales and that the vibrational mode mixing produces a dipole reorientation ($\pi/2$ jumps) on the same time scale as observed in the pump−probe anisotropy.

Frequency−Frequency Correlation Function (FFCF). The 2D IR spectrum contains some of the characteristics of the FFCF such as correlation times and amplitudes. The correlation decay for times longer than ca. 200 fs can be obtained from the slope of the nodal line, separating the positive and negative peaks of the 2D IR spectrum.[29] To characterize the dynamics of the degenerate asymmetric

dx.doi.org/10.1021/jp3069333 | J. Phys. Chem. B 2013, 117, 4354−4364

transitions of TCM^- ion, the waiting time evolution of slope (Figure 10) was measured at the point of intersection with the line joining the positive and negative peaks.

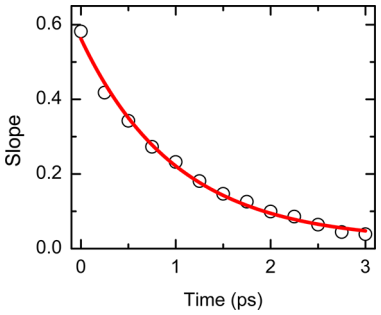

Figure 10. Slope, $S(T)$, versus waiting time, T. The open circles are the experimental data points, and the solid line is a fit to the data points corresponding to an exponential decay.

The experimental slope suggests a model function of the form: $S(T) = a_1 \exp(-T/\tau_1) + a_2$ where the first component has a decay constant of 1.1 ps with an amplitude of 0.54. The second component has an amplitude of 0.04 and does not decay within the longest waiting time measured, suggesting the presence of a small slower inhomogeneous component which is too long to be resolved within the time scale of the experiments. Moreover, the correlation time τ_1 is approximately twice that of the fast component of the anisotropy decay which suggests that the mechanism by which the frequency is dephased is different from the process responsible for the anisotropy decay.

The frequency-frequency correlation function for each of the nearly degenerate pair of transitions of the TCM^- ion was also evaluated from the instantaneous frequencies (see the Theoretical Methodologies section). The frequency correlation function shows that each of the A modes present an oscillatory term that is slowly damped exponentially (eq 10).

$$\langle \delta\omega_i(0)\delta\omega_i(t)\rangle = Ae^{-t/\tau_c}\sin(2\pi c\tilde{\nu}t) \quad (10)$$

The FFCF for modes A1 and A2 fit well to a frequency ($\tilde{\nu}$) of 2544 cm^{-1} and a correlation constant (τ_c) of 1.3 ps. There is also a small contribution from a mode at 780 cm^{-1}, which has a frequency similar to the in plane bending of the CN groups and is not considered in the FFCF analysis. The damping time constant, which represents the decay time of the frequency correlations, is very similar to the frequency−frequency correlation time observed experimentally from the 2D IR slope as indicated in Figure 11. The similarity between theoretical and experimental FFCF correlation times suggests that this quantity is properly characterized from 2D IR spectra even when interstate energy transfer is taking place in the system. Thus, this result reinforces the idea that the ultrafast anisotropy and FFCF decays are solvent induced processes that may arise from different types of solvent interactions. It will be seen that the symmetry of the TCM^- ion makes possible a distinction between the two processes.

2D IR Spectra Simulation. The model used here for the 2D IR spectral simulation has been described in detail elsewhere.[8] This model accounts for the energy transfer between the one-quantum modes by allowing spontaneous jumps from one state to the other during the waiting time (T), which are incorporated in the simulation by using multiplicative

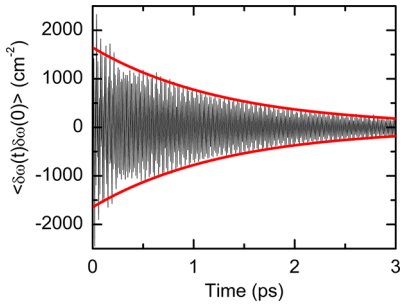

Figure 11. Frequency−frequency autocorrelation function corresponding to mode A1. The red lines are constructed using fitting parameters to help visualizing the fitting with eq 10.

factors of $P_{11}(T)$ and $P_{12}(T)$. However, it does not include any coherence transfer process during the τ and t times. The orientational factors for XXXX polarizations for each of the pathways and their dependence on the rotational diffusion coefficient for a symmetric top diffuser have been tabulated previously and have been employed in the simulation. The vibrational frequency autocorrelation functions for both the components of the degeneracy are assumed to be Kubo functions: $C(t) = \Delta^2 e^{-t/\tau_c}$, where Δ and τ_c are the fluctuation amplitude and the frequency−frequency autocorrelation time respectively. Similarly the vibrational cross-correlation function for both the transitions are also assumed to be the same and have the following form: $C_{ij}(t) = fC(t)$ where f represents the correlation coefficient. The parameters used for the 2D IR absorptive spectra simulation have been listed in Table 1. The parameters not directly observed in the experiment, such as frequencies of the modes (ω_1 and ω_2), etc., were selected in such a way that they reproduce the 2D IR and linear IR absorption spectra. For example, a correlation coefficient, f, of 0.5 was selected because it produces the best match to the experimental 2D IR spectra. The remaining parameters used in the simulation of the 2D IR spectra are those obtained from the experiments.

Figure 6 shows the simulated absorptive 2D IR spectra at different waiting times (T = 0−3 ps) based on the parameters listed in Table 1. Although the simulated spectra do not exactly reproduce the observed 2D IR spectra, they capture the major features of the experimentally obtained 2D IR absorptive spectra such as their upright and "square like" shape of the spectra at higher waiting time. These spectral features corroborate the presence of underlying cross-peaks between the two nearly degenerate states at later values of T. Also, the cross-peak to diagonal peak ratio obtained from the signal across a trace perpendicular to the diagonal and passing through the maximum has a waiting time dependence similar to that obtained experimentally (see the Supporting Information). In addition, the waiting time dynamics of the slope of the zeroth contour line was measured from the simulated 2D IR spectra. As in the experiment, the calculated slope decays exponentially with a characteristic time of 1.1 ps (see the Supporting Information). These similarities between parameters obtained from the experimental and simulated 2D IR spectra not only support the model of energy transfer and vibrational dephasing presented in the previous sections but also validate the experimental procedures for obtaining dynamics parameters from the 2D IR, such as the energy transfer rate.

dx.doi.org/10.1021/jp3069333 | J. Phys. Chem. B 2013, 117, 4354−4364

Hydration Dynamics. The frequencies observed are characteristic of nitrile groups so the A1, A2, and S modes of the TCM^- ion are mainly localized in the CN groups (Figure 2). Therefore water molecules directly in contact with the nitrile groups will be the ones most likely to bring about the loss in correlation of the A1 and A2 transition frequencies. If those same water motions were to dominate the population transfer between the degenerate states, both processes might be expected to present a similar time evolution. However, the TCM^- ion exhibits a frequency correlation time which is slower by a factor of two than that observed for the anisotropy decay suggesting that the faster reorientation of the transition dipoles in the TCM^- ion is produced by a different subset of water motions or interactions between water and the ion for which the time scales for energy transfer and the frequency fluctuation correlations need not be the same. For example it can be imagined that water molecules hydrogen bonding exactly along the CN axis might not cause complete averaging of the directions of the transition dipoles in the plane, whereas the same motions may cause large frequency fluctuations. There might also be an interaction between the negatively charged central carbon and a hydrogen atom of water. However the dominant nitrile frequency fluctuations may not be strongly correlated to weak solvation of the central carbon since the displacement of the central atom makes only a small contribution to these degenerate normal modes (Figure 2). Furthermore water molecules atop the TCM^- ion will break the symmetry and localize the transition dipoles. Another possible mechanism of dipole localization is bending of a single C−C−N bond, which will break the symmetry of the ion and induce the mode mixing. As shown later, this deformation does not produce large frequency shifts or splitting of the degenerate mode. These possibilities need to be tested using simulations and quantum chemical computations aimed at interpreting the origin of the two time scales, the causes of the energy transfer, and why the frequency fluctuations are slower.

The potential energy surface along the energy minimum pathway for the TCM^- ion−water complex was evaluated using DFT computations of the energy as a function of the distance between the central carbon atom and the oxygen of the water. The ab initio potential (Figure 12) shows two minima: a local

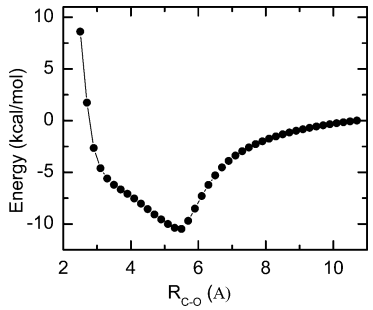

Figure 12. Potential of TCM^- as a function of the distance between the oxygen atom of a water molecule and the central carbon of TCM^-.

minimum at 3.5 Å and a global minimum at 5.5 Å. The optimized geometries show that the global minimum has the water hydrogen bonded to one CN group but the minimum located at 3.5 Å has the water H-bonded to the central carbon atom. Thus, the interaction of water with the central carbon atom is energetically favorable. In addition, the radial distribution functions computed from the MD simulation show that the CN groups are H-bonded during most of the simulation time and that the central carbon atom also has H-bond interactions although much less frequently (Figure 13).

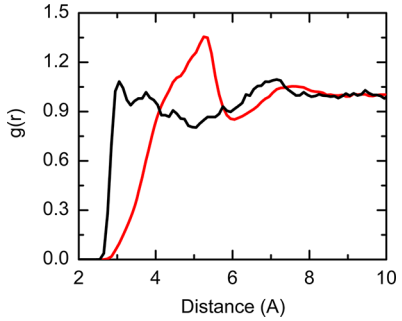

Figure 13. Radial distribution function plot, $g_{C(TCM^-)-O(water)}(r)$ (red) and $g_{N(TCM^-)-O(water)}(r)$ (black) obtained from MD simulation where $C(TCM^-)$ represents the central carbon and $N(TCM^-)$ represents one of the terminal nitrogen atoms.

The ratio of the average number of H-bonds, as defined below, at the terminal nitrogen atoms and the central carbon atom is 6:1 which agrees with the ratio of probabilities of water at H-bond distance observed from the radial distribution functions in Figure 13 (g_{N-Ow} (3 Å)/g_{C-Ow} (3.5 Å) ≈ 1/0.2).

The central carbon H-bond dynamics was extracted from the MD simulation by using the standard parameters for a hydrogen bond[30] (see the Supporting Information). The time correlation function (Figure 14) of the number of H-bonds

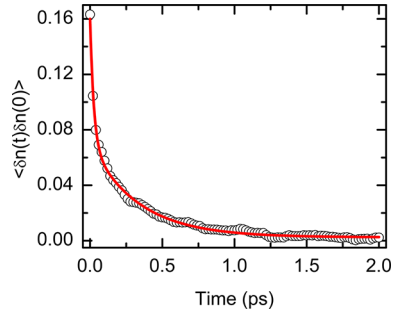

Figure 14. Time correlation function for H-bond number fluctuation with one of the central carbon.

with the central carbon ($\langle \delta n(t)\ \delta n(0)\rangle$ where $\delta n(t) = n(t) - \langle n(t)\rangle$) can be described with two components, one with a very fast decay time constant of 25 fs and the other with a time constant of 0.35 ps. Although the fast decay time can be associated with the libration motion of water that breaks the H-bond while maintaining the actual position of the water molecule, the slow time constant is a measure of local H-bond moving in and out of the top/bottom region of the ion is similar to the ultrafast decay time of the anisotropy (0.58 ps) and may contribute to the population transfer. In addition, ab initio calculations show that a water molecule H-bonded to the central carbon atom with a particular orientation relative to the TCM^- ion plane (Figure 15) would influence the directions of the dipoles of the two transitions to the degenerate level. Also, these computations predict a frequency splitting of less than 10 cm^{-1} between the A1 and A2 states when a water molecule is H-bonded to the central carbon atom, which is not inconsistent with the observed frequency separation (Table 1).

dx.doi.org/10.1021/jp3069333 | J. Phys. Chem. B 2013, 117, 4354−4364

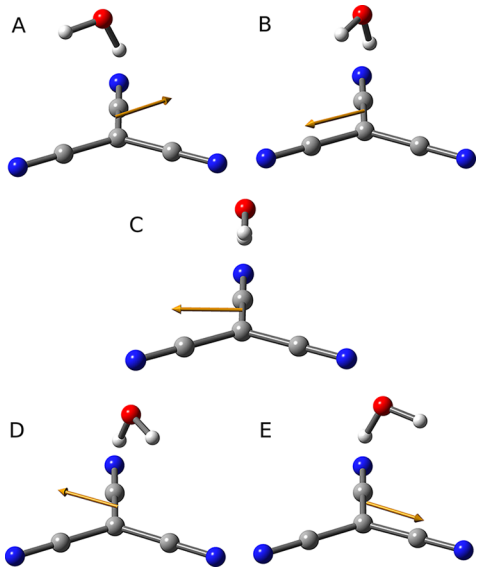

Figure 15. Transition dipole orientation of TCM^- with water H-bonded in different orientations. The panels A, B, C, D, and E show water molecule with 0°, 30°, 60°, 90°, and 120° of the dihedral angle formed by the left C−C bond and the H−O bond of water closest to the ion. The golden arrows represent the transition dipole direction for the A1 mode of TCM^- ion.

A water molecule H-bonded to the central carbon would cause transition dipole reorientations, but this is not the only possible source of mode mixing. The interaction of water with only one CN group of the molecule would also cause symmetry breaking particularly if the H-bond bends the C−C−N bond. DFT calculations show that the energy required for bending the C−C−N bond is less than 3 kcal/mol for bending angles of less than 15°. In addition, an analysis of the MD simulation, containing all possible thermal motions, indicates that the in plane bending of the C−C−N bond has a correlation decay time of 0.3 ps (not shown), which is very similar to the dynamics of the population transfer. Moreover, DFT calculations predict that the frequency fluctuations of the degenerate mode caused by these motions are very small (10 cm^{-1} for a 14° bend having a probability of occurrence of ca. 0.06) suggesting they make a negligible contribution to the frequency fluctuation correlation function. Because the degenerate modes are composed of linear combinations of the CN stretches (Figure 2), "collective" motions of waters interacting with the CN stretches may be important in causing the significant frequency variations. An analysis of these collective motions of water is beyond the scope of the present work and will be dealt with in a future publication.

CONCLUSION

The nearly degenerate asymmetric stretch transition of the TCM^- ion at 2172 cm^{-1} in water shows solvent induced population transfer on ultrafast time scales (~0.6 ps), which leads to very fast decay in the pump−probe anisotropy and causes the appearance of overlapping cross-peaks in the 2D IR absorptive spectrum as a function of waiting time. In addition the TCM^- ion undergoes vibrational frequency dephasing more slowly than the transition dipole reorientational relaxation. This result suggests that the two processes involve different hydration mechanisms. Molecular dynamics simulations and ab initio computations have been employed to examine the different types of water interactions. They provide molecular pictures of processes in which the frequency relaxation is determined by the immediate solvation shell of the nitrile groups. On the other hand, the subpicosecond transition dipole reorientation motion is caused by the interaction with water molecules that break the 3-fold symmetry, such as those H-bonding to the central carbon atom and those causing C−C−N bending. A transition dipole reorientation mechanism induced by the interaction of a CN group with a single water molecule might prevail in some of the other high-symmetry systems mentioned earlier.[7−11]

ASSOCIATED CONTENT

Supporting Information

Comparison between bleach/stimulated emission and new absorption pump−probe data, the comparison between experimental and simulated 2D IR data, and the description of some theoretical methodologies. This material is available free of charge via the Internet at http://pubs.acs.org.

AUTHOR INFORMATION

Corresponding Author

*E-mail: hochstra@sas.upenn.edu.

Author Contributions

[†]D.G.K. and P.K.S. contributed equally to this work.

Notes

The authors declare no competing financial interest.

[‡]On leave from Bhabha Atomic Research Centre, Trombay, Mumbai 400085, India.

ACKNOWLEDGMENTS

This research was supported by Grants to R.M.H. from NSF-CHE and NIH-GM12592 and NIH-RR001348/9P41GM104605 for instrumentation.

REFERENCES

(1) Aliaga, C.; Baldelli, S. *J. Phys. Chem. C* **2008**, *112*, 3064.
(2) Wang, P.; Zakeeruddin, S. M.; Gratzel, M.; Kantlehner, W.; Mezger, J.; Stoyanov, E. V.; Scherr, O. *Appl. Phys. A: Mater. Sci. Process.* **2004**, *79*, 73.
(3) Kim, S. Y.; Kim, S.; Park, M. J. *Nat. Comm.* **2010**, *1*, 88.
(4) Weidinger, D.; Houchins, C.; Owrutsky, J. C. *Chem. Phys. Lett.* **2012**, *525*−*526*, 60.
(5) Long, D. A.; Carrington, R. A. G.; Gravenor, R. B. *Nature* **1962**, *196*, 371.
(6) Kuroda, D. G.; Hochstrasser, R. M. *Phys. Chem. Chem. Phys.* **2012**, *14*, 6219.
(7) Vorobyev, D. Y.; Kuo, C.-H.; Chen, J.-X.; Kuroda, D. G.; Scott, J. N.; Vanderkooi, J. M.; Hochstrasser, R. M. *J. Phys. Chem. B* **2009**, *113*, 15382.
(8) Vorobyev, D. Y.; Kuo, C. H.; Kuroda, D. G.; Scott, J. N.; Vanderkooi, J. M.; Hochstrasser, R. M. *J. Phys. Chem. B* **2010**, *114*, 2944.
(9) Kuroda, D. G.; Hochstrasser, R. M. *J. Chem. Phys.* **2011**, *135*, 204502.
(10) Sando, G. M.; Zhong, Q.; Owrutsky, J. C. *J. Chem. Phys.* **2004**, *121*, 2158.
(11) Tokmakoff, A.; Fayer, M. D. *J. Chem. Phys.* **1995**, *103*, 2810.
(12) Kim, Y. S.; Wang, J. P.; Hochstrasser, R. M. *J. Phys. Chem. B* **2005**, *109*, 7511.
(13) Case, D. A.; Darden, T. A.; Cheatham, T. E. I.; Simmerling, C. L.; Wang, J.; Duke, R. E.; Luo, R.; Merz, K. M.; Pearlman, D. A.; Crowley, M. et al. AMBER 9, 9th ed.; University of California: San Francisco, CA, 2006.

(14) Wilson, E. B.; Decius, J. C.; Cross, P. C. *Molecular Vibrations*; Dover Publications, Inc.: Mineola, NY, 1980.
(15) Kabsch, W. *Acta Crystallogr.* **1978**, *A34*, 827.
(16) Sisak, D.; McCusker, L. B.; Buckl, A.; Wuitschik, G.; Wu, Y. L.; Schweizer, W. B.; Dunitz, J. D. *Chem.—Eur. J.* **2010**, *16*, 7224.
(17) Mukamel, S. *Principles of nonlinear optical spectroscopy*; Oxford University Press: New York, 1995.
(18) Kuroda, D. G.; Hochstrasser, R. M. Polarization anisotropy effects for degenerate vibrational levels. In *Ultrafast Infrared Vibrational Spectroscopy*; Fayer, M. D., Ed.; CRC Press: Boca Raton, FL, 2012 (in press).
(19) Hu, C. M.; Zwanzig, R. *J. Chem. Phys.* **1974**, *60*, 4354.
(20) Sension, R. J.; Hochstrasser, R. M. *J. Chem. Phys.* **1993**, *98*, 2490.
(21) Sension, R. J.; Repinec, S. T.; Szarka, A. Z.; Hochstrasser, R. M. *J. Chem. Phys.* **1993**, *98*, 6291.
(22) Ghosh, A.; Tucker, M. J.; Hochstrasser, R. M. *J. Phys. Chem. A* **2011**, *115*, 9731.
(23) Hamm, P.; Zanni, M. T. *Concepts and Methods of 2D Infrared Spectroscopy*; Cambridge University Press: Cambridge, U.K., 2011.
(24) Cho, M. H. *Two-Dimensional Optical Spectroscopy*; CRC Press: Boca Raton, FL, 2009.
(25) Tucker, M. J.; Gai, X. S.; Fenlon, E. E.; Brewer, S. H.; Hochstrasser, R. M. *Phys. Chem. Chem. Phys.* **2011**, *13*, 2237.
(26) Kuroda, D. G.; Vorobyev, D. Y.; Hochstrasser, R. M. *J. Chem. Phys.* **2010**, *132*, 044501.
(27) Kozinski, M.; Garrett-Roe, S.; Hamm, P. *Chem. Phys.* **2007**, *341*, 5.
(28) Oxtoby, D. W. *J. Chem. Phys.* **1979**, *70*, 2605.
(29) Kwac, K.; Cho, M. H. *J. Chem. Phys.* **2003**, *119*, 2256.
(30) Luzar, A.; Chandler, D. *Nature* **1996**, *379*, 55.